https://doi.org/10.5194/egusphere-2025-6055
Preprint. Discussion started: 12 December 2025

High-Latitude Eddy Statistics from SWOT assessed by *in situ* observations

Charly de Marez[1], Arne Bendinger[1], and Ahmad Fehmi Dilmahamod[2]

[1]Laboratoire d'Océanographie Physique et Spatiale, Univ. Brest, CNRS, Ifremer, IRD, IUEM, Plouzané, France
[2]GEOMAR Helmholtz Centre for Ocean Research, Kiel, Germany

Correspondence: Charly de Marez (charly.demarez@univ-brest.fr)

Abstract.

Mesoscale eddies play a key role in the transport of heat, salt, and momentum, yet their statistical characterization at high latitudes has remained elusive due to the coarse resolution of conventional satellite altimetry. Here we present the first statistical description of mesoscale eddies in the Labrador Sea using observations from the Surface Water and Ocean Topography (SWOT) mission. We apply an eddy-detection algorithm directly to the native 2-km SWOT swaths, without gridding or assimilation, and validate the detections against *in situ* measurements from shipboard current profiler data from one cruise in 2024, as well as against a statistically derived shipboard current-profiler–based eddy census. The comparison demonstrates excellent agreement in eddy size and intensity, confirming SWOT's ability to resolve high-latitude mesoscale structures previously undetectable in gridded altimetry. The SWOT-derived eddy census based on a full-calendar year reveals a predominance of energetic anticyclones (Irminger Rings) in the basin interior and smaller cyclones along the continental slopes, with clear seasonal variability linked to boundary current instability. These findings provide the first observational benchmark for mesoscale activity in the Labrador Sea and illustrate SWOT's potential to extend eddy statistics to high-latitude and ice-influenced regions, opening the way for a global assessment of mesoscale variability.

1 Introduction

Mesoscale eddies are ubiquitous features of the world ocean, playing a fundamental role in the transport of heat, salt, and nutrients, as well as in the redistribution of momentum and energy across spatial scales (Chelton et al., 2011; Zhang et al., 2014; Dong et al., 2014). Given their widespread influence, detecting and characterizing mesoscale eddies at the global scale has long been a key objective of physical oceanography.

Over the past two decades, automatic eddy detection has been made possible through the availability of global gridded sea level anomaly (SLA) products derived from conventional nadir altimetry (see all literature from Chelton et al., 2007). These datasets have allowed systematic eddy tracking and the construction of global eddy atlases. However, these products are fundamentally limited by their spatial resolution, usually 1/4° or 1/8°, which constrains their ability to resolve eddies smaller than ~ 50 km in diameter (Ballarotta et al., 2019). Gridded SLA fields have previously been questioned in accurately representing the eddy field resulting in largely distorted eddy characteristics (Amores et al., 2018). This is linked to the spatio-temporal

https://doi.org/10.5194/egusphere-2025-6055
Preprint. Discussion started: 12 December 2025

interpolation during the mapping procedure which compromises the scales to be resolved and sampling capabilities (Le Traon et al., 1998; Pujol et al., 2016). Validation of such large-scale eddy datasets remains sparse, as direct *in situ* observations suitable for comparison are rare and spatially limited. Furthermore, a major blind spot persists *at high latitudes* ($> 50°$N/S), where the first baroclinic Rossby radius of deformation (R_D) is only a few tens of kilometers (de Marez et al., 2025), well below the resolving capacity of conventional altimetry (Amores et al., 2018).

Yet, mesoscale dynamics at high latitudes play a critical role in shaping water mass transformation and air–sea heat exchange, notably within subpolar gyres and regions of deep convection (Beaird et al., 2016). Eddies mediate restratification after winter convection, influence deep-water formation, and contribute to the variability of boundary currents (Rieck et al., 2019; Du Plessis et al., 2019; Zhang et al., 2022). They are particularly abundant in two dynamical environments: the marginal ice zone (MIZ) and the unstable coastal currents that border subpolar basins. In the MIZ, sea-ice melt generate sharp density gradients that trigger geophysical instabilities and lead to intense eddy formation; these eddies, often organized as dipoles, actively disperse sea-ice floes and contribute to the widening of the ice edge region (Manucharyan and Thompson, 2017; Manucharyan et al., 2022). Their associated heat fluxes also accelerate sea-ice melt by transporting warm, saline waters toward the surface and poleward (Thompson et al., 2014; Si et al., 2023). This results in a positive feedback between eddy activity and sea-ice retreat: the more eddies, the more sea ice melts (Manucharyan and Thompson, 2022). However, because of their small spatial scales and the scarcity of *in situ* observations, the statistical properties of high-latitude eddies remain poorly constrained, leaving a major gap in our understanding of polar and subpolar ocean dynamics.

Here, we take advantage of the unprecedented capabilities of the Surface Water and Ocean Topography (SWOT) wide-swath altimeter to bridge this gap. For the first time, SWOT allows us to resolve and characterize mesoscale eddies at high latitudes with a resolution fine enough to capture the relevant spatial scales. Using SWOT 2-km sea level anomaly swaths, we develop and apply an eddy-detection methodology specifically designed to preserve small-scale variability and to quantify eddy statistics. We focus on the Labrador Sea, where SWOT-derived eddy characteristics can be validated against independent and statistically robust *in situ* measurements from the shipboard surveys described in Bendinger et al. (2025). This latter study provides a uniquely comprehensive, ship-based census of mesoscale and submesoscale eddies in the central Labrador Sea, offering an ideal reference for assessing SWOT's performance. In parallel, recent work by Jensen et al. (2025) has demonstrated SWOT's ability to reveal mesoscale features at such high latitudes (in another region, the East Greenland Shelf). While their study focuses on the detailed characterization of SLA snapshots and relies primarily on SST for validation, our approach extends this capability toward a quantitative and statistically grounded assessment of the eddy field at high latitude, supported by a dedicated *in situ* reference dataset.

This study presents the first statistical description of mesoscale eddies at high latitude, in the Labrador Sea, from wide-swath satellite observations. Section 2 describes the data. Section 3 presents the methodology of the SWOT-based detections and its validation against *in situ* observations. Section 4 discusses the spatial and temporal variability of eddy characteristics in the Labrador Sea, and Section 5 discusses and summarizes the main findings of the study.

https://doi.org/10.5194/egusphere-2025-6055
Preprint. Discussion started: 12 December 2025

2 Data

2.1 SWOT data

We leverage SWOT satellite data (see some background in *e.g.,* Morrow et al., 2019). We use the latest release (v2.0.1) of Level-3 SWOT data, namely the SWOT_L3_SSH 'Basic' (2-km resolution) product, derived from the L3 SWOT Ka-band Radar Interferometer (KaRIn) Low rate ocean data products provided by NASA/JPL and CNES. The Level-3 processing removes SWOT's systematic errors, and has been extensively validated using other altimeters, numerical models, and *in situ* data, in the global ocean (Dibarboure et al., 2025). These datasets are produced and freely distributed by the AVISO and DUACS teams as part of the DESMOS Science Team project (AVISO/DUACS, 2023).

Here, we use the "filtered" Sea Level Anomaly (SLA) variable. The filtering procedure is described in Tréboutte et al. (2023). It is based on a U-Net–based convolutional neural network, trained on simulated North Atlantic data, and shown to outperform classical filtering methods. The method reduces significantly the noise (by a factor of 2), while preserving the balance part of the signal at spatial scales down to 10 km (Demol et al., submitted). This method allows to extract most of the balanced signal out of the full SSH signal, but it tends to reduce the overall energy, which complicates the interpretation in lower-energy regions due to the noise levels (see *e.g.,* Callies and Wu, 2019). However, this has no implications for our analysis, as we focus on the mesoscale signal, and recent studies have revealed SWOT's ability to resolve mesoscale structures that were previously undetected in gridded products (Zhang et al., 2024a, b; Verger-Miralles et al., 2025; Du and Jing, 2024; Damerell et al., 2025; Wang et al., 2025; Tchilibou et al., 2025; Carli et al., 2025; Dibarboure et al., 2025; Zhang et al., 2025; de Marez et al., 2025; Archer et al., 2025)

We consider data during the "science phase" (with a 21-day repeat orbit), from cycle #9 to cycle #26, covering the period from 5th January 2024 to 31st December 2024, thus the whole seasonal cycle of year 2024. We extract SWOT measurement in the Labrador Sea area, which represent 74 SWOT passes in total (see one cycle of measurement in the area of interest in Fig. 1).

2.2 SADCP data

We complement the SWOT satellite observations with ship-based velocity measurements obtained from Shipboard Acoustic Doppler Current Profilers (SADCPs). SADCPs provide high-resolution profiles of horizontal current velocity along the ship track by measuring the Doppler shift of acoustic signals reflected by waterborne scatterers. The instruments operated at frequencies between 38 kHz and 150 kHz, providing near-surface velocity estimates at an along-track resolution of roughly 200–300 m. SADCP data collected during MSM129 in June-July 2024 aboard the RV Maria S. Merian is used, with the instrument operating at 75 kHz, and providing near-surface velocity estimates at an along-track resolution of roughly 200-300 m. The data were processed following the same procedure as for MSM74, as detailed in Bendinger et al. (2025). The processed ship-based velocity measurements were then used to fit idealized eddy solutions along the SADCP transects, allowing reconstructions of eddy centers and key dynamical properties (see Bendinger et al. (2025) for methodological details). These reconstructions provide a robust *in situ* "truth" against which we can directly assess the performance and reliability of the SWOT-based eddy

https://doi.org/10.5194/egusphere-2025-6055
Preprint. Discussion started: 12 December 2025

detection, enabling a direct comparison of mesoscale eddy structures between SWOT and MSM129 (Fig. 2). In addition, we compare the statistical results of Bendinger et al. (2025), which are based on SADCP observations from the MSM40, MSM54, and MSM74 cruises and comprise 40 well-resolved eddies with radii of 3–39 km and azimuthal velocities of 7–58 cms^{-1}, with the SWOT-based statistics, as shown in the histograms in Fig. 3.

Eddy detection statistics from a classical 1/4° satellite altimetry are also used for comparison purpose. The detection is the one performed in Bendinger et al. (2025), and is referred to as "CMEMS" for Copernicus Marine Environment Monitoring Service in *e.g.,* Fig. 3b,d. Note that these eddy statistics are only representative of eddies along or close to the ship tracks of MSM40, MSM54, and MSM74 campaigns.

2.3 Other dataset

We use the sea ice concentration from the OSI SAF dataset (https://doi.org/10.48670/moi-00134), and the ETOPO Global Relief Model dataset (https://doi.org/10.25921/fd45-gt74) to assess respectively the sea ice concentration, and the depth at each eddy location.

https://doi.org/10.5194/egusphere-2025-6055
Preprint. Discussion started: 12 December 2025

3 Eddy detection from non-interpolated SWOT data

3.1 The methodology

Each SWOT pass consists of two adjacent swaths, each approximately 50 km wide, resulting in a combined swath width of about 120 km. These swaths are separated by a nadir gap of approximately 20 km, where no—KaRIn—measurements are collected. See for example the "raw" pass #563 of cycle #10 in the top left of Fig. 1. The swaths are oriented along the satellite's ground track, providing detailed across-track coverage. Within each pass, the measurement grid is composed of 69 across-track pixels, and N along-track pixels, with each pixel representing a 2 km by 2 km area on the Earth's surface. Measurement gaps can occur within the swaths due to various factors, including rain cells which can attenuate the radar signal and lead to missing data in certain regions, or sea ice for example.

We apply an eddy-detection procedure directly on the 2-km resolution swath product of SWOT, without performing any subsequent gridded assimilation, in contrast to classical gridded altimetric product based eddy detection approaches, that now include SWOT measurements (see *e.g.,* Gómez-Navarro et al., 2025, who used the Experimental multimission gridded L4 sea level heights and velocities with SWOT KaRIn data, MIOST). Working in the native swath geometry maximizes our ability to identify small-scale features that might otherwise be lost in the smoothing and gridding stages of standard products. Additionally, the mesoscale eddies in our high-latitude study region are smaller than this swath width, hence an eddy can typically wholly be contained within a single swath pass — enabling reliable detection and sizing. The procedure is as follows (see also Fig. 1 for an example):

We use the native 2-km resolution SWOT swaths, which have a width of 69 pixels across-track. To facilitate processing, each swath is first padded at the edges (step #1 in Fig. 1a) and then divided into overlapping 128×128 pixel windows with a 64-pixel overlap (step #2 in Fig. 1a). This produces SLA sub-images containing NaN gaps, which are subsequently filled using a biharmonic inpainting method, yielding complete 128×128 pixel SLA images (step #3 in Fig. 1a). Specifically, the `inpaint_biharmonic` function from the python `skimage.restoration` module was used. This later reconstructs missing values by solving the biharmonic equation ($\nabla^4 u = 0$) within the regions of missing data. This technique ensures a smooth interpolation by minimizing the Laplacian of the interpolated field, producing a physically consistent and continuous surface that preserves the mesoscale eddies structure and allows closed contours to form even across the gap between the two swaths.

Eddies are then identified in each sub-image using the `py-eddy-tracker` package (Mason et al., 2014), and filtered using a set of predefined criteria to ensure robustness (step #4 in Fig. 1a). First, a maximum of 40% of the eddy contour (defined by the region of maximum azimuthal velocity) is allowed to overlap with gaps in the SLA field, preventing spurious features generated by the inpainting procedure. This condition is suppressed when the eddy center lies near the middle of the pass (in the gap between swaths) and a tolerance of 60% of gaps is then allowed. Finally, only eddies exceeding a minimum radius of 5 km and a minimum amplitude of 0.01 m are retained. These criteria ensure that the detected features correspond to physically meaningful mesoscale structures within the SWOT swaths. Note that sensitivity tests to this parameters were done to choose their values—low variability of probability distributions were obtained from these sensitivity tests. The remaining

https://doi.org/10.5194/egusphere-2025-6055
Preprint. Discussion started: 12 December 2025

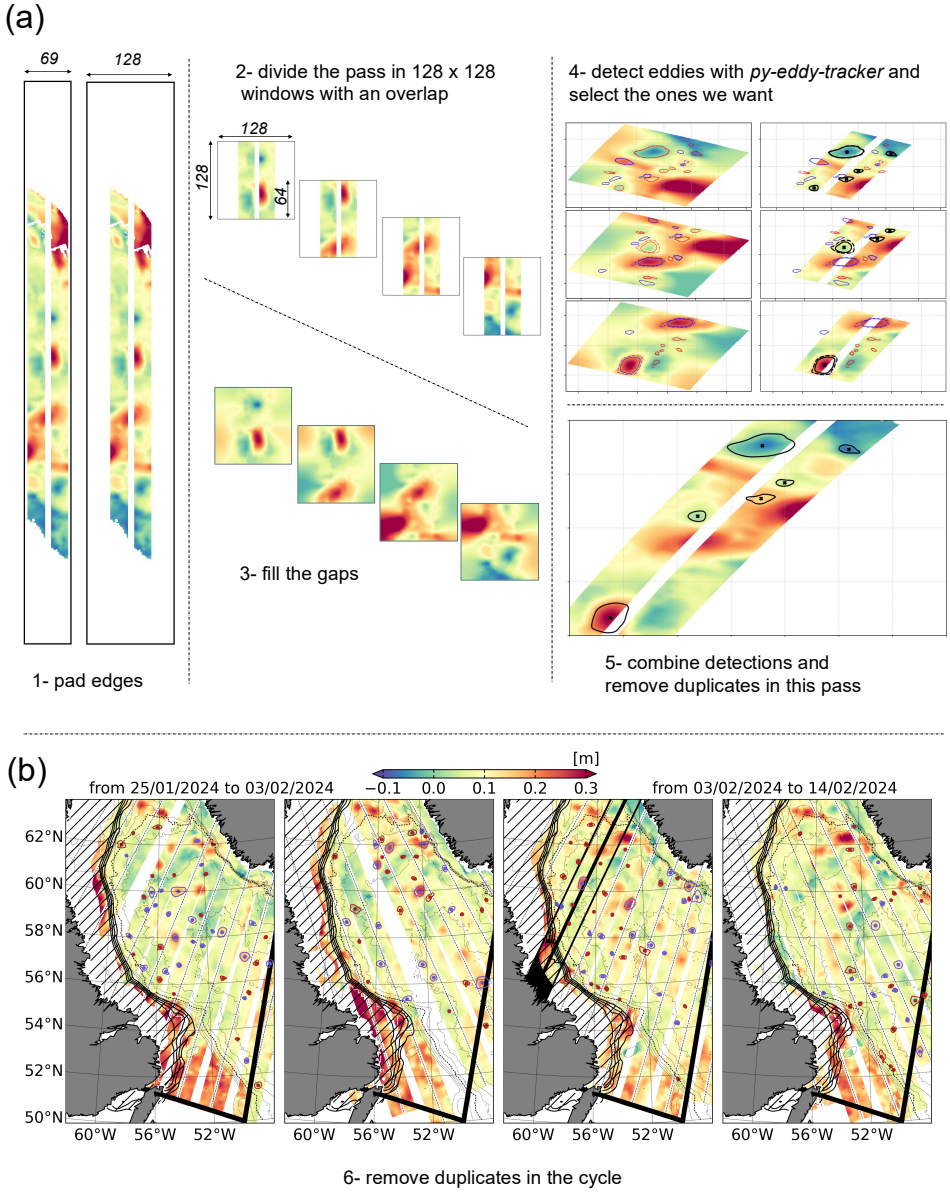

Figure 1. a) Example of the detection methodology in pass #563, and cycle 10. b) Mesoscale eddy detection in the Labrador Sea from non-interpolated SWOT data for cycle 10; blue (resp. red) contours (resp. dots) indicate anticyclonic (resp. cyclonic) eddy contours of maximum velocity (resp. centers); thin contours indicate isobaths every 500 m (dotted line highlights isobath 2000 m); thick contours indicate the average sea ice concentration in the period of the map every 10% (the $> 10\%$ area is hatched); the pass #563 shown in panel a is highlighted in the third panel.

https://doi.org/10.5194/egusphere-2025-6055
Preprint. Discussion started: 12 December 2025

eddy arrays from all sub-images are merged, with duplicates in the overlapping regions removed, providing a complete set of eddy detections for each SWOT pass (step #5 in Fig. 1a).

Finally, for each cycle, duplicates are removed by identifying eddies whose centers are separated by a distance shorter than their radius of maximum velocity (hereafter radius or $\mathrm{R_{max}}$ for conciseness) and a distance threshold of 10 km. This threshold corresponds to the typical displacement of an eddy advected by Rossby wave propagation over one SWOT repeat cycle. Eddies detected at a position where sea ice concentration is larger than 15% are removed. Further, for the comparison with ship-derived eddy characteristics (see Section 2.2 and 3.2), we only consider eddy detections at depths larger than 2000 m to solely focus on eddies in the central Labrador Sea, similarly to Bendinger et al. (2025). This gives for each SWOT cycle all detected eddies in the area of interest (see Fig. 1b). It is important to note that an eddy may be re-detected in successive cycles; therefore, this methodology does not provide the absolute number of eddies, but rather a *detection probability per cycle*. The method may also detect a few submesoscale vortices where R_D is large, but these cases fall near the mesoscale–submesoscale transition ($R/R_D \sim 1$; see Fig. 3). We therefore treat all detections as mesoscale eddies in this study.

https://doi.org/10.5194/egusphere-2025-6055
Preprint. Discussion started: 12 December 2025

3.2 Validation of the method in front of *in situ* data

Validating the eddy detection method requires comparing the eddy characteristics obtained from SWOT data with independent *in situ* observations of eddies in the same region: this comparison must rely on another source of measurement, with eddy statistics derived from an alternative detection approach. However, establishing a suitable ground truth is not straightforward. On one hand, classical gridded altimetry products cannot serve as a reference, since their coarse resolution and interpolation algorithm prevent them from resolving mesoscale eddies in high-latitude regions (Amores et al., 2018; Bendinger et al., 2025). On the other hand, one could consider using eddies detected from high-resolution numerical simulations or reanalyses, either directly on their native grid or by simulating SWOT-like tracks and applying the same detection algorithm. Yet, such an approach would implicitly assume that the model perfectly represents the mesoscale dynamics of the region—an assumption that has not itself been validated, leading to a circular argument.

During the MSM129 cruise conducted in spring 2024 in the Labrador Sea, four anticyclonic mesoscale eddies (hereafter A_{1-4}) were sampled with the SADCP. The specific track crossing the eddies, as well as their associated surface velocity fields (averaged between 22 m and 102 m depth), are shown in Fig. 2a,d,e. We take advantage of the method developed by Bendinger et al. (2025) and applied it to this specific dataset, from which the main dynamical properties of the eddies are retrieved to validate the outcome of our SWOT-eddy detection method. The findings are summarized in the table in Fig. 2f.

All four eddies were successfully captured in coincident SWOT passes and detected by our SWOT-based eddy detection method. The eddies identified in SWOT exhibit radii and maximum azimuthal velocities that are in good agreement with those measured during the MSM129 cruise. It is important to note that the SWOT detections and the *in situ* observations were not made at the same time. For instance, A_1 was observed *in situ* on 24 June 2024, while its SWOT counterpart was detected on 27 June 2024 (it was also identified on 25 June and 6 July but duplicate detections across cycles were automatically removed; see Fig. 2a–c). The slight reduction in velocity amplitude seen in the SWOT data can be attributed to the instrument's spatial smoothing, which tends to dampen kinetic energy. Also, SWOT altimetry measures an integrated quantity, which tends to be weaker than directly measured surface velocity from SADCP directly. Nevertheless, the close spatial coincidence between eddy centers and contours identified by the two independent approaches, together with their comparable dynamical characteristics, confirms the robustness and reliability of our detection algorithm when applied to the native 2-km SWOT swath data.

To assess the robustness of our detection method at the statistical level, we use the comprehensive *in situ* dataset published by Bendinger et al. (2025), which provides a unique reference for eddy statistics in the Labrador Sea. Using their *in situ* methodology, a large number of mesoscale and submesoscale eddies were identified and characterized, allowing the construction of histograms of the main eddy dynamical properties — including radius, maximum azimuthal velocity, and Rossby number. This dataset thus represents an unprecedented "ground truth" for the eddy field in this high-latitude region, against which we can directly compare the SWOT-based results. The distributions obtained from SWOT detections show remarkable agreement with the *in situ* statistics, both in terms of typical eddy scales and dynamical intensity, see Fig. 3. In contrast, the eddy statistics derived from CMEMS gridded altimetry display much larger radii and weaker velocities, reflecting the well-known smoothing and scale limitations of mapped altimetry products at these latitudes. When including shallow eddies detected above

https://doi.org/10.5194/egusphere-2025-6055
Preprint. Discussion started: 12 December 2025

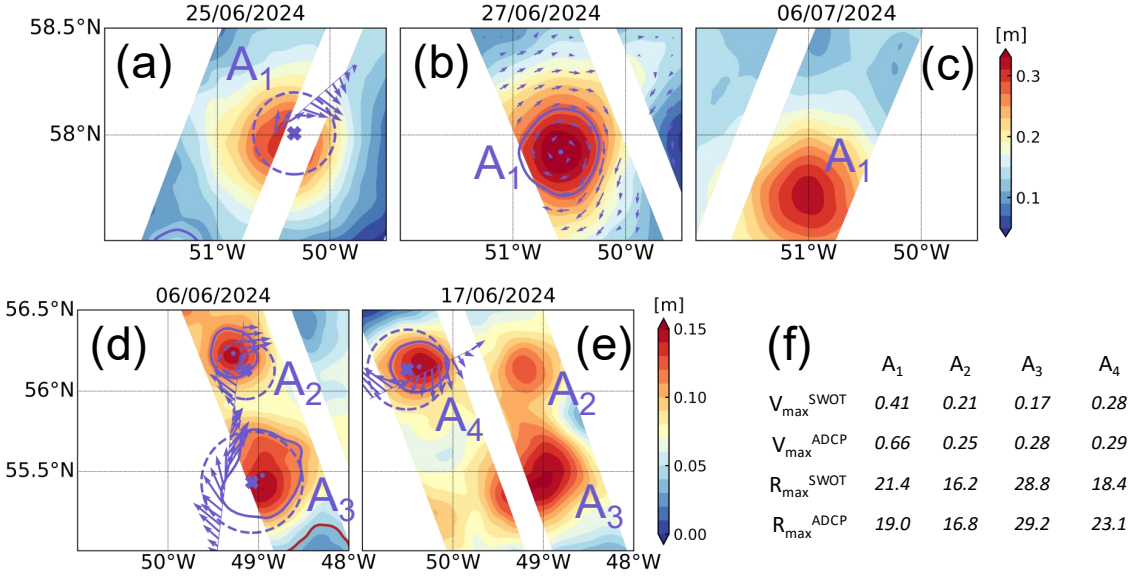

Figure 2. Comparison between eddy detections in SWOT altimetry data and the eddy identification method of Bendinger et al. (2025) applied to observations from the 2024 MSM129 cruise in the Labrador Sea, where four eddies were observed. Panels (a–e) show the sea level anomaly (SLA) from SWOT, over which detected eddies are mapped. In panels (b, d, e), solid lines indicate the maximum azimuthal velocity contours of SWOT-detected eddies, and dots mark their centers. Panel (b) also shows the geostrophic velocity field derived from SWOT. In panels (a, d, e), crosses indicate the centers of eddies identified during MSM129, with circles marking their radii; arrows show the surface velocity from the SADCP, used for the *in situ* eddy identification along the ship's trajectory. Eddies $A_{1\text{-}4}$ correspond to the four observed structures. Their maximum velocity (in $\mathrm{m\,s^{-1}}$) and radius (in km) are summarized in panel (f) for both SWOT detections and SADCP identifications.

depth < 2000 m, we find an increased number of small-radius eddies, consistent with the reduced Rossby deformation radius on the continental shelf, but reaching the limitations of SWOT capabilities.

With the *in situ* validation confirming the reliability and robustness of our detection approach, we can confidently apply it and analyze eddies detected using SWOT in the Labrador Sea. In the following section, we examine the eddy field observed in the Labrador Sea throughout 2024, focusing on the spatial distribution and dynamical characteristics of the detected eddies. This provides the first spatial statistical description of the regional mesoscale activity at such high latitude.

https://doi.org/10.5194/egusphere-2025-6055
Preprint. Discussion started: 12 December 2025

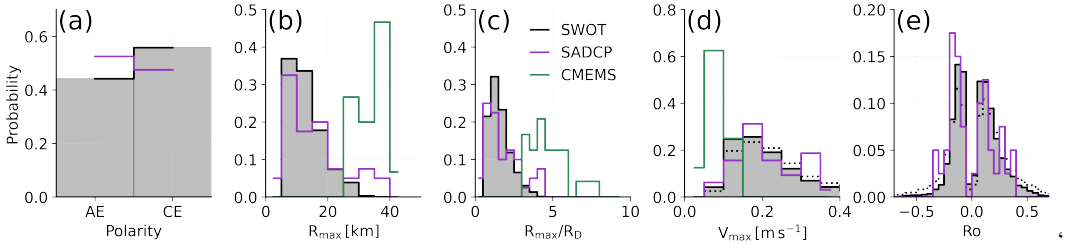

Figure 3. Probability distribution of eddy statistics detected by SWOT (gray bars, solid black lines) in comparison with ADCP (purple) and CMEMS (green) a) Polarity of detected eddies, expressed as the proportion of anticyclonic (AE) and cyclonic (CE) structures. b) Distribution of radius of maximum azimuthal velocity $\mathrm{R_{max}}$. c) Distribution of $\mathrm{R_{max}}$ normalized by the first baroclinic deformation radius $\mathrm{R_D}$. d) Distribution of maximum azimuthal velocity $\mathrm{V_{max}}$. e) Distribution of the Rossby number Ro of detected eddies. In panels c and d, dotted lines are distributions including all detections prior to depth filtering (*i.e.*, $<$ 2000 including eddies on shelves).

4 Eddy characteristics in the Labrador Sea during year 2024

The spatial distribution and dynamical characteristics of eddies detected in the Labrador Sea during 2024 are shown in Fig. 4. Anticyclonic eddies (AEs, Fig. 4a–d) are widespread across the basin. They are detected both along the continental slopes and within the deep interior. Their distribution is relatively homogeneous in the central and western Labrador Sea, with enhanced activity near the 3000–3500 m isobaths where mesoscale instabilities of the boundary currents are expected. In contrast, cyclonic eddies (CEs, Fig. 4e–h) are more frequently observed along the continental slopes, particularly in regions influenced by the West Greenland and Labrador Currents, where intense shear and topographic steering promote cyclonic vorticity generation (Chanut et al., 2008; Thomsen et al., 2014; Pacini and Pickart, 2022). This pattern is also found in Fu et al. (2025): they also detected cyclonic eddies in the eastern Labrador Sea from conventional altimetry.

The observed AE/CE asymmetry likely reflects the greater propagation range of anticyclones. AEs are less susceptible to steering by background currents and less prone to instability-driven decay, enabling them to travel farther into the basin interior compared to the more rapidly disrupted CEs.

Eddies exhibit radii of maximum velocity ($\mathrm{R_{max}}$) ranging between 5 and 34 km, with an average (standard deviation) value of 15(6) km for AEs, and 11(5) km for CEs. The prevalence of large, energetic AEs in the basin interior is consistent with the presence of Irminger Rings (de Jong et al., 2014), which detach from the boundary current system and propagate westward into the convective region. Along the continental slopes, both eddy types display higher maximum velocities and elevated Rossby numbers, reflecting the enhanced strain and frictional interactions with the topography. In these regions, the flow can locally depart from geostrophic balance (Ro$\sim$ 1), challenging the assumptions made in our methodology.

The delineated boxes in Fig. 4 (black contours) show the sub-regions used to compute the time series of eddy occurrence and mean properties shown in Fig. 5.

In the western area, both eddy types exhibit fairly constant radii of maximum velocity $\mathrm{R_{max}} \sim 10$km, but with noticeably higher velocities ($\mathrm{V_{max}} \sim 0.3-0.4\,\mathrm{m\,s^{-1}}$) and Rossby numbers (Ro$\sim$0.3) in late winter and spring. This period coincides with

https://doi.org/10.5194/egusphere-2025-6055
Preprint. Discussion started: 12 December 2025

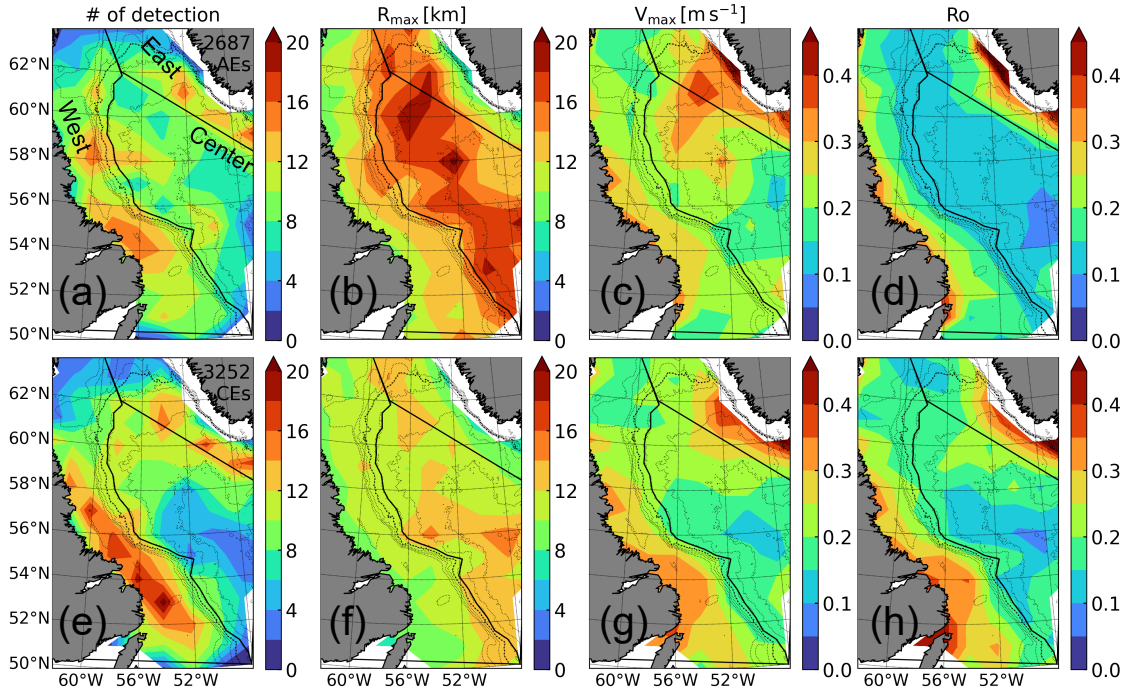

Figure 4. a) Number of detected anticyclonic eddies (AEs) in $2^\circ \times 1^\circ$ boxes during year 2024; each eddy is unique within the cycle it is detected in, but can be re-detected the next cycle as no tracking is performed. b,c,d) Bin-averaged radius of maximum velocity $\mathrm{R_{max}}$, maximum velocity $\mathrm{V_{max}}$, and Rossby number Ro of detected AEs. e,f,g,h) Same as panels a,b,c,d but for cyclonic eddies (CEs). Black solid lines indicate the delimitation of areas for the computation of timeseries shown in Fig. 5. Same isobaths as in Fig. 1b are shown.

the peak of baroclinic instability along the West Greenland Current, which favors the generation of energetic boundary eddies (with slightly smaller $\mathrm{R_{max}}$).

In the central Labrador Sea, $\mathrm{R_{max}}$ and $\mathrm{V_{max}}$ for AEs increase markedly from spring to early autumn, reaching values near 18–20 km and $0.3\,\mathrm{m\,s^{-1}}$, respectively. This seasonal strengthening reflects the westward propagation and growth of Irminger Rings as they move into the convective basin, leading to eddy-induced re-stratification after winter deep mixing. Cyclonic eddies, by contrast, remain weaker and smaller throughout the year, consistent with their local generation by shear and topographic interactions.

In the eastern area, eddy properties show larger variability and weaker seasonality. Both AE and CE radii remain around 10–15 km, while velocities seldomly exceed $0.25\,\mathrm{m\,s^{-1}}$. This pattern likely reflects the dominance of small, topographically trapped vortices and the limited mesoscale energy input in the eastern basin.

Overall, throughout 2024, clear regional and temporal contrasts emerge between AEs and CEs. The time series reveal a pronounced seasonal cycle of mesoscale activity: eddies are more energetic during late winter–spring, when baroclinic instability and boundary current variability peak there (see Rieck et al., 2019), and weaken toward autumn, following the re-stratification.

https://doi.org/10.5194/egusphere-2025-6055
Preprint. Discussion started: 12 December 2025

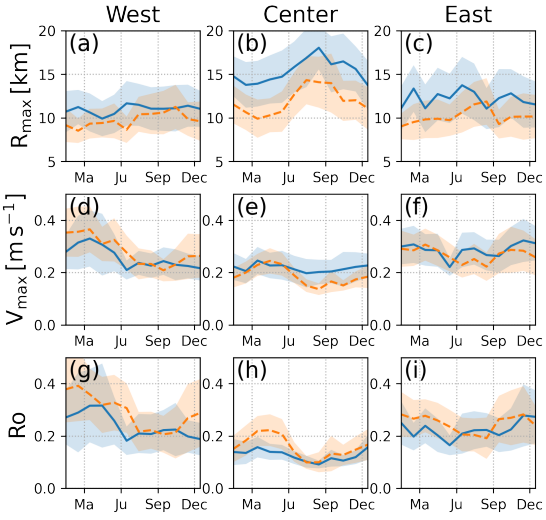

Figure 5. a,b,c) Monthly-averaged R_{max} in the West, Center, and East areas, respectively, for AEs (blue) and CEs (orange) during year 2024; areas are defined in Fig. 4; envelopes show the standard deviation. d,e,f) Same as panels a,b,c but for V_{max}. g,h,i) Same as panels a,b,c but for Ro.

The evolution of AE properties in particular highlights the continuous formation, detachment, and westward spreading of Irminger Rings across the Labrador Sea —a process now observed synoptically for the first time with SWOT.

https://doi.org/10.5194/egusphere-2025-6055
Preprint. Discussion started: 12 December 2025

5 Discussion

In the last two decades, a broad range of (surface-intensified) eddy types have been identified in the Labrador Sea: Irminger Rings, convective lenses, and boundary current eddies, that feature radii in the range of 5-35 km. These observations mostly relied on mooring observations (*e.g.,* Lilly and Rhines, 2002), conventional altimetry (Fu et al., 2025), numerical models (Rieck et al., 2019) or sparse hydrographic sections, which limited the ability to assess eddy statistics or their variability. Here, we provide the first statistically robust description of mesoscale eddies (in the 5-35 km radius range) in the Labrador Sea derived solely from satellite observations. Our SWOT-based detections offers a continuous and quantitative view of the mesoscale field, resolving structures that conventional gridded altimetry could not capture.

The observed eddy characteristics are consistent with previous regional studies describing the prevalence of anticyclonic Irminger Rings and the smaller, topographically constrained cyclones along the continental slopes (de Jong et al., 2014; Pacini and Pickart, 2022). SWOT reveals their full spatial extent and intensity, showing that the mesoscale field is more energetic and heterogeneous than inferred from existing products. By resolving eddies down to scales of a few kilometers, SWOT bridges the gap between *in situ* observations and large-scale altimetric analyses, offering a new framework to evaluate eddy–convection coupling and boundary current instabilities in subpolar regions. The strong consistency between SWOT and *in situ* eddy properties validates the approach and provides an observational benchmark for future modelling and reanalysis efforts.

Beyond the Labrador Sea, these results highlight SWOT's transformative potential for observing mesoscale and submesoscale dynamics in high-latitude and coastal environments. Its fine spatial resolution and direct swath observations overcome the scale limitations of conventional altimetry, allowing the detection of eddies of size comparable to the local Rossby radius of deformation with reliable estimates of radius, velocity, and amplitude.

These findings set the stage for the construction of global SWOT-based eddy climatologies, extending into subpolar and seasonally ice covered zones where altimetric data were previously unusable. The Labrador Sea serves as a prototype of such regions, combining strong boundary current variability, deep convection, and seasonal sea-ice influence. Ultimately, SWOT provides a means to quantify how mesoscale turbulence contributes to poleward heat transport and sea-ice variability — a key component of ocean–climate feedbacks.

https://doi.org/10.5194/egusphere-2025-6055
Preprint. Discussion started: 12 December 2025

Code and data availability. SWOT data can be downloaded on AVISO website https://www.aviso.altimetry.fr/en/my-aviso-plus.html.

Author contributions. CDM conceptualized the study, developed the eddy detection method from SWOT data, and conducted the analysis. AB developed the eddy characterization method from *in situ* data and provided its outputs from MSM40, MSM54, and MSM74 campaigns. AFD conducted the analysis of MSM129 campaign. CDM, AB, and AFD wrote the manuscript.

Competing interests. The authors declare no competing interests.

Acknowledgements. CDM acknowledges support from the Centre National de la Recherche Scientifique (CNRS). AB was funded by the Centre National d'Études Spatiales (CNES) and supported by the French national program LEFE/GMMC (Les Enveloppes Fluides et l'Environnement/Groupe Mission Mercator Coriolis). AFD acknowledges support from the European ObsSea4Clim project. ObsSea4Clim "Ocean observations and indicators for climate and assessments" is funded by the European Union, Horizon Europe Funding Programme for Research and Innovation under grant agreement number: 101136548. ObsSea4Clim contribution nr. 36

https://doi.org/10.5194/egusphere-2025-6055
Preprint. Discussion started: 12 December 2025

References

Amores, A., Jordà, G., Arsouze, T., and Le Sommer, J.: Up to what extent can we characterize ocean eddies using present-day gridded altimetric products?, Journal of Geophysical Research: Oceans, 123, 7220–7236, https://doi.org/10.1029/2018JC014140, 2018.

Archer, M., Wang, J., Klein, P., Dibarboure, G., and Fu, L.-L.: Wide-swath satellite altimetry unveils global submesoscale ocean dynamics, Nature, 640, 691–696, 2025.

AVISO/DUACS: SWOT Level-3 SSH Unsmoothed (v2.0.1) [Data set], https://doi.org/0.24400/527896/A01-2024.003, 2023.

Ballarotta, M., Ubelmann, C., Pujol, M.-I., Taburet, G., Fournier, F., Legeais, J.-F., Faugère, Y., Delepoulle, A., Chelton, D., Dibarboure, G., et al.: On the resolutions of ocean altimetry maps, Ocean science, 15, 1091–1109, 2019.

Beaird, N., Rhines, P., and Eriksen, C.: Observations of seasonal subduction at the Iceland-Faroe Front, Journal of Geophysical Research: Oceans, 121, 4026–4040, 2016.

Bendinger, A., Dilmahamod, A. F., Albert, A., Le Sommer, J., and Karstensen, J.: Characteristics of Mesoscale-to-Submesoscale Eddies in the Labrador Sea: Insights from Ship Observations, Journal of Physical Oceanography, 55, 2037–2057, https://doi.org/10.1175/JPO-D-24-0216.1, 2025.

Callies, J. and Wu, W.: Some Expectations for Submesoscale Sea Surface Height Variance Spectra, Journal of Physical Oceanography, 49, 2271–2289, 2019.

Carli, E., Tranchant, Y., Siegelman, L., Le Guillou, F., Morrow, R. A., Ballarotta, M., and Vergara, O.: Small-scale eddy diagnostics around the Southern Ocean Polar Front with SWOT, Authorea Preprints, 2025.

Chanut, J., Barnier, B., Large, W., Debreu, L., Penduff, T., Molines, J. M., and Mathiot, P.: Mesoscale eddies in the Labrador Sea and their contribution to convection and restratification, Journal of Physical Oceanography, 38, 1617–1643, https://doi.org/10.1175/2008JPO3485.1, 2008.

Chelton, D. B., Schlax, M. G., Samelson, R. M., and de Szoeke, R. A.: Global observations of large oceanic eddies, Geophysical Research Letters, 34, https://doi.org/10.1029/2007GL030812, 2007.

Chelton, D. B., Gaube, P., Schlax, M. G., Early, J. J., and Samelson, R. M.: The Influence of Nonlinear Mesoscale Eddies on Near-Surface Oceanic Chlorophyll, Science, 334, 328–332, https://doi.org/10.1126/science.1208897, 2011.

Damerell, G. M., Bosse, A., and Fer, I.: Merging of a mesoscale eddy into the Lofoten Vortex in the Norwegian Sea captured by an ocean glider and SWOT observations, EGUsphere, 2025, 1–28, 2025.

de Jong, M., Bower, A., and Furey, H.: Two years of observations of warm-core anticyclones in the Labrador Sea and their seasonal cycle in heat and salt stratification, Journal of Physical Oceanography, 44, 427–444, https://doi.org/10.1175/JPO-D-13-070.1, 2014.

de Marez, C., Vives, C. R., Portela, E., and Ruiz-Angulo, A.: Mesoscale ocean processes: The critical role of stratification in the Icelandic region, Journal of Geophysical Research: Oceans, 130, e2025JC022 664, 2025.

Demol, M., Ponte, A., Garreau, P., Bellacicco, M., Berta, M., Centurioni, L., Doglioli, A., Joel, A., Mourre, B., and Pascual, A.: Large Drifter Experiment in the Western Mediterranean Sea reveals Dynamical vs Noise contributions in SWOT-KaRIn Sea Level, Geophysical Research Letters, submitted.

Dibarboure, G., Anadon, C., Briol, F., Cadier, E., Chevrier, R., Delepoulle, A., Faugère, Y., Laloue, A., Morrow, R., Picot, N., et al.: Blending 2D topography images from the Surface Water and Ocean Topography (SWOT) mission into the altimeter constellation with the Level-3 multi-mission Data Unification and Altimeter Combination System (DUACS), Ocean Science, 21, 283–323, 2025.

https://doi.org/10.5194/egusphere-2025-6055
Preprint. Discussion started: 12 December 2025

Dong, C., McWilliams, J. C., Liu, Y., and Chen, D.: Global heat and salt transports by eddy movement, Nature Communications, 5, https://doi.org/10.1038/ncomms4294, 2014.

Du, T. and Jing, Z.: Fine-Scale Eddies Detected by SWOT in the Kuroshio Extension, Remote Sensing, 16, 3488, 2024.

Du Plessis, M., Swart, S., Ansorge, I. J., Mahadevan, A., and Thompson, A. F.: Southern ocean seasonal restratification delayed by submesoscale wind–front interactions, Journal of Physical Oceanography, 49, 1035–1053, 2019.

Fu, C., Müller, V., and Myers, P. G.: Large Mesoscale Eddy Properties and Dynamics in the Labrador Sea from Satellite Altimetry, Atmosphere-Ocean, 63, 334–352, 2025.

Gómez-Navarro, L., Ballarotta, M., Cortés-Morales, D., Pujol, M.-I., Fortunato, L., Mourre, B., and Pascual, A.: New insights on mesoscale activity in the western Mediterranean Sea, State of the Planet Discussions, 2025, 1–22, https://doi.org/10.5194/sp-2025-17, 2025.

Jensen, S., Andersen, O., Ludwigsen, C., Gonçalves-Araujo, R., and de Steur, L.: Surface water and ocean topography (SWOT) observations unveil small mesoscale variability on the East Greenland shelf, Geophysical Research Letters, 52, e2025GL118 573, 2025.

Le Traon, P. Y., Nadal, F., and Ducet, N.: An Improved Mapping Method of Multisatellite Altimeter Data, Journal of Atmospheric and Oceanic Technology, 15, 522–534, https://doi.org/10.1175/1520-0426(1998)015<0522:AIMMOM>2.0.CO;2, 1998.

Lilly, J. M. and Rhines, P. B.: Coherent eddies in the Labrador Sea observed from a mooring, Journal of Physical Oceanography, 32, 585–598, https://doi.org/10.1175/1520-0485(2002)032<0585:CEITLS>2.0.CO;2, 2002.

Manucharyan, G. E. and Thompson, A. F.: Submesoscale sea ice-ocean interactions in marginal ice zones, Journal of Geophysical Research: Oceans, 122, 9455–9475, 2017.

Manucharyan, G. E. and Thompson, A. F.: Heavy footprints of upper-ocean eddies on weakened Arctic sea ice in marginal ice zones, Nature communications, 13, 2147, 2022.

Manucharyan, G. E., Lopez-Acosta, R., and Wilhelmus, M. M.: Spinning ice floes reveal intensification of mesoscale eddies in the western Arctic Ocean, Scientific Reports, 12, 7070, 2022.

Mason, E., Pascual, A., and McWilliams, J. C.: A new sea surface height–based code for oceanic mesoscale eddy tracking, Journal of Atmospheric and Oceanic Technology, 31, 1181–1188, 2014.

Morrow, R., Fu, L.-L., Ardhuin, F., Benkiran, M., Chapron, B., Cosme, E., d'Ovidio, F., Farrar, J. T., Gille, S. T., Lapeyre, G., et al.: Global observations of fine-scale ocean surface topography with the Surface Water and Ocean Topography (SWOT) mission, Frontiers in Marine Science, 6, 232, 2019.

Pacini, A. and Pickart, R. S.: Meanders of the west Greenland current near cape farewell, Deep Sea Research Part I: Oceanographic Research Papers, 179, 103 664, https://doi.org/10.1016/j.dsr.2021.103664, 2022.

Pujol, M.-I., Faugère, Y., Taburet, G., Dupuy, S., Pelloquin, C., Ablain, M., and Picot, N.: DUACS DT2014: the new multi-mission altimeter data set reprocessed over 20 years, Ocean Science, 12, 1067–1090, https://doi.org/10.5194/os-12-1067-2016, 2016.

Rieck, J. K., Böning, C. W., and Getzlaff, K.: The nature of eddy kinetic energy in the Labrador Sea: Different types of mesoscale eddies, their temporal variability, and impact on deep convection, Journal of Physical Oceanography, 49, 2075–2094, 2019.

Si, Y., Stewart, A. L., and Eisenman, I.: Heat transport across the Antarctic Slope Front controlled by cross-slope salinity gradients, Science Advances, 9, eadd7049, 2023.

Tchilibou, M., Carrere, L., Lyard, F., Ubelmann, C., Dibarboure, G., Zaron, E. D., and Arbic, B. K.: Internal tides off the Amazon shelf in the western tropical Atlantic: analysis of SWOT Cal/Val mission data, Ocean Science, 21, 325–342, 2025.

Thompson, A. F., Heywood, K. J., Schmidtko, S., and Stewart, A. L.: Eddy transport as a key component of the Antarctic overturning circulation, Nature Geoscience, 7, 879–884, 2014.

https://doi.org/10.5194/egusphere-2025-6055
Preprint. Discussion started: 12 December 2025

Thomsen, S., Eden, C., and Czeschel, L.: Stability analysis of the Labrador Current, Journal of Physical Oceanography, 44, 445–463, https://doi.org/10.1175/JPO-D-13-0121.1, 2014.

Tréboutte, A., Carli, E., Ballarotta, M., Carpentier, B., Faugère, Y., and Dibarboure, G.: KaRIn noise reduction using a convolutional neural network for the SWOT ocean products, Remote Sensing, 15, 2183, 2023.

Verger-Miralles, E., Mourre, B., Gómez-Navarro, L., Barceló-Llull, B., Casas, B., Cutolo, E., Díaz-Barroso, L., d'Ovidio, F., Tarry, D. R., Zarokanellos, N. D., et al.: SWOT enhances small-scale eddy detection in the Mediterranean Sea, Geophysical Research Letters, 52, e2025GL116 480, 2025.

Wang, J., Archer, M., Klein, P., and Fu, L.-L.: Global Submesoscale Ocean Dynamics Unveiled by Wide-Swath Satellite Altimetry, 2025.

Zhang, L., Liu, C., Sun, W., Wang, Z., Liang, X., Li, X., and Cheng, C.: Modeling Mesoscale Eddies Generated Over the Continental Slope, East Antarctica, Frontiers in Earth Science, 10, 970, 2022.

Zhang, L., Hwang, C., Liu, H.-Y., Chang, E. T., and Yu, D.: Automated Eddy Identification and Tracking in the Northwest Pacific Based on Conventional Altimeter and SWOT Data, Remote Sensing, 17, 1665, 2025.

Zhang, X., Liu, L., Fei, J., Li, Z., Wei, Z., Zhang, Z., Jiang, X., Dong, Z., and Xu, F.: Advances in Surface Water and Ocean Topography for Fine-Scale Eddy Identification from Altimeter Sea Surface Height Merging Maps, EGUsphere, 2024, 1–19, 2024a.

Zhang, Z., Wang, W., and Qiu, B.: Oceanic mass transport by mesoscale eddies, Science, 345, 322–324, https://doi.org/10.1126/science.1252418, 2014.

Zhang, Z., Miao, M., Qiu, B., Tian, J., Jing, Z., Chen, G., Chen, Z., and Zhao, W.: Submesoscale eddies detected by SWOT and moored observations in the Northwestern Pacific, Geophysical Research Letters, 51, e2024GL110 000, 2024b.